# Atomic Structure and Kinetics of NASICON $Na_xV_2(PO_4)_3$ Cathode for Sodium-Ion Batteries

*Zelang Jian, Chenchen Yuan, Wenze Han, Xia Lu, Lin Gu,* Xuekui Xi,* Yong-Sheng Hu,* Hong Li, Wen Chen, Dongfeng Chen, Yuichi Ikuhara, and Liquan Chen*

**$Na_3V_2(PO_4)_3$ is one of the most important cathode materials for sodium-ion batteries, delivering about two Na extraction/insertion from/into the unit structure. To understand the mechanism of sodium storage, a detailed structure of rhombohedral $Na_3V_2(PO_4)_3$ and its sodium extracted phase of $NaV_2(PO_4)_3$ are investigated at the atomic scale using a variety of advanced techniques. It is found that two different Na sites (6b, M1 and 18e, M2) with different coordination environments co-exist in $Na_3V_2(PO_4)_3$, whereas only one Na site (6b, M1) exists in $NaV_2(PO_4)_3$. When Na is extracted from $Na_3V_2(PO_4)_3$ to form $NaV_2(PO_4)_3$, $Na^+$ occupying the M2 site (CN = 8) is extracted and the rest of the Na remains at M1 site (CN = 6). In addition, the Na atoms are not randomly distributed, possibly with an ordered arrangement in M2 sites locally for $Na_3V_2(PO_4)_3$. $Na^+$ ions at the M1 sites in $Na_3V_2(PO_4)_3$ tend to remain immobilized, suggesting a direct M2-to-M2 conduction pathway. Only Na occupying the M2 sites can be extracted, suggesting about two Na atoms able to be extracted from the $Na_3V_2(PO_4)_3$ structure.**

## 1. Introduction

Lithium resource is limited and unevenly distributed in a few countries, while sodium is the sixth richest element and widely distributed on the earth, suggesting that sodium-ion batteries are more sustainable, crust and economical than lithium-ion batteries for large-scale stationary batteries.[1] An increasing number of researchers are realizing the importance of sodium-ion batteries. Numerous electrode materials for sodium-ion batteries have been tested in the last few years.[1,2] $Na_3V_2(PO_4)_3$ with NASICON structure, which has large interstitial channels for fast $Na^+$ ion migration,[3] shows a very flat voltage curve with a plateau at around 3.4 V *vs.* $Na^+$/Na (similar as the plateau voltage of $LiFePO_4$ *vs.* $Li^+$/Li) and superior electrochemical performance. The capacity is about 107 mAh/g, which corresponds to approximate two Na extraction/insertion from/into the structure.[3b,4] The structure evolution of the $Na_3V_2(PO_4)_3$ electrode during cycling is a typical two-phase transformation between $Na_3V_2(PO_4)_3$ and $NaV_2(PO_4)_3$.[4] Part of Na atoms remains in the lattice, which cannot be completely extracted from the structure by the electrochemical method, even with charge voltage as high as 4.5 V vs. $Na^+$/Na (Figure S1). Thus, chemical oxidation method was carried out alternatively. However, X-ray diffraction (XRD) results (Figure S2) show that when excess strong oxidant $NO_2BF_4$ is employed, $NaV_2(PO_4)_3$, rather than $V_2(PO_4)_3$ is obtained. In addition, when the ratio of $NO_2BF_4$: $Na_3V_2(PO_4)_3$ is 1, a mixture with $Na_3V_2(PO_4)_3$ and $NaV_2(PO_4)_3$ is obtained, confirming that two Na can be easily extracted and the third one is difficult to be extracted from the $Na_3V_2(PO_4)_3$ structure. The $Na^+$ ion diffusion mechanism in this type NASICON structured material is still in dispute.[3a,5] To further understand the structure evolution and mechanism of $Na^+$ ion diffusion, it is necessary to characterize the local structure and dynamics at atomic scale, whereas it remains a challenge.[6]

Rietveld method is a well-established technique for quantitative phase analysis that is successfully used with X-ray diffraction (XRD) data.[7] The application of XRD Rietveld method to lithium/sodium-ion battery for structure analysis,[8] has provided insight into mechanism of lithium/sodium storage. Aberration-corrected annular-bright-field (ABF) scanning transmission electron microscopy (STEM) provides a feasible access to a direct interpretation of the atomic structure at sub-angstrom resolution. ABF-STEM has been successfully applied to observe lithium ions in $LiFePO_4$,[9] $Li_4Ti_5O_{12}$[10] and so on.[11] Compared with lithium ion, sodium ion has a lager radius and larger scattering cross-sections for electrons, allowing it to be readily seen in ABF-STEM. Solid-state $^{6,7}$Li nuclear magnetic resonance (NMR) spectroscopy is a routine method for characterizing

Dr. Z. L. Jian, Dr. C. C. Yuan, Dr. X. Lu, Prof. L Gu, Prof. X. K. Xi, Prof. Y.-S. Hu, Prof. H. Li, Prof. L. Q. Chen
Beijing National Laboratory for Condensed Matter Physics
Institute of Physics
Chinese Academy of Sciences
Beijing 100190, China
E-mail: l.gu@iphy.ac.cn; xi@iphy.ac.cn; yshu@aphy.iphy.ac.cn
Dr. Z. L. Jian, Prof. W. Chen
School of Materials Science and Engineering
Wuhan University of Technology
Wuhan 430070, China
Dr. W. Z. Han, Prof. D. F. Chen
China Institute of Atomic Energy
Beijing 102413, China
Prof. Y. Ikuhara
Institute of Engineering Innovation
University of Tokyo
Tokyo 113–8654, Japan

**DOI: 10.1002/adfm.201400173**

the local structure and dynamics of Li ions in crystalline or amorphous solids, which cannot be easily accessed by conventional structural and electrochemical approaches.[12] However, $^{23}$Na NMR studies are hampered by the reduced resolution due to the larger quadrupole broadening. Furthermore, the existence of magnetic moment from redox active center yields very short relaxation times which are even less than the correlation times of ion exchange process,[13] making it difficult to gain microscopic information on ion motions.[14]

Here, in order to understand the mechanism of sodium storage in $Na_3V_2(PO_4)_3$, we combined the above mentioned techniques to study the structure evolution and kinetics from $Na_3V_2(PO_4)_3$ to $NaV_2(PO_4)_3$ by preparing chemically sodium-extracted $Na_3V_2(PO_4)_3$. We identified the information of sodium's occupancy in $Na_3V_2(PO_4)_3$ and $NaV_2(PO_4)_3$. The evolution of sodium's occupancy was directly observed by ABF-STEM. Then we used NMR to probe sodium site structure at room temperature. Na nuclei spin dynamics and magnetic properties at various temperatures were also investigated from the analysis of $^{23}$Na NMR line shifts and line shapes.

## 2. Results and Discussion

### 2.1. Rietveld Refined-XRD

**Figure 1** shows the Rietveld-refined X-ray diffraction patterns of $Na_3V_2(PO_4)_3$ and $NaV_2(PO_4)_3$ obtained at room temperature. The crystal parameters are summarized in **Table 1**, **Table 2**, and Table S1. It can be seen that $Na_3V_2(PO_4)_3$ sample is a single phase and well crystallized. All the diffraction peaks are indexed in a rhombohedral system with the space group of $R\bar{3}c$. The structure is built on a 3D framework of $VO_6$ octahedra sharing all the corners with $PO_4$ tetrahedra (Figure S3). Two octahedral $VO_6$ connected with three tetrahedral $PO_4$ constitute a basic unit named as a lantern. Each lantern is connected with six other lanterns, generating a large interstitial space that can accommodate sodium ions. The reliability factors are very good ($R_p$ = 3.30, $R_{wp}$ = 4.22 and $R_{exp}$ = 1.93). The unit cell parameters are indicated as follows: a = 8.738 Å and c = 21.815 Å. In order to clarify the occupancy of Na sites, the atom positions and occupancy were refined. The results (Table 1) show two different occupancies of Na sites: 6b sites ($Na_1$, M1) and 18e sites ($Na_2$, M2). The corresponding occupancy rates are 0.8430 (M1 sites) and 0.7190 (M2 sites), respectively. Numerous vacancies offer the channel of Na ion transport, resulting in classical NASICON structure.[15] It is very interesting to find that the occupancy rate is highly dependent on the temperature as shown in Table S1. For instance, at 100 K, the corresponding occupancy rates are 1 (M1 sites) and 0.667 (M2 sites), respectively. With the decrease of temperature, the lattice of $Na_3V_2(PO_4)_3$ shrinks a little bit (see Table S2), in this case, Na is possibly more thermodynamically favorable occupying the M1 site which has smaller polyhedral volume than that of M2 site (see Table S3). Therefore, part of Na at M2 site will be driven to adjacent M1 site at a lower temperature until the occupancy at M1 site is 1. The chemically sodium extracted sample $NaV_2(PO_4)_3$ based on $Na_3V_2(PO_4)_3$ shows different XRD patterns. $NaV_2(PO_4)_3$ is a single phase and well crystallized, too. It still remains the rhombohedral structure with the space group of $R\bar{3}c$. The unit cell parameters are as follows: a = 8.426 Å and c = 21.720 Å. The volume decreases because of the sodium extraction from $Na_3V_2(PO_4)_3$ and this change is only by 8.26%. Rietveld refined-XRD results (Table 2) exhibit that the reliability factors are as follows: $R_p$ = 7.17, $R_{wp}$ = 10.3 and $R_{exp}$ = 4.39. In $NaV_2(PO_4)_3$, Na occupies only one site (M1), whose occupancy rate increases to 0.9448, whereas no Na atom occupies any M2 site. It indicates

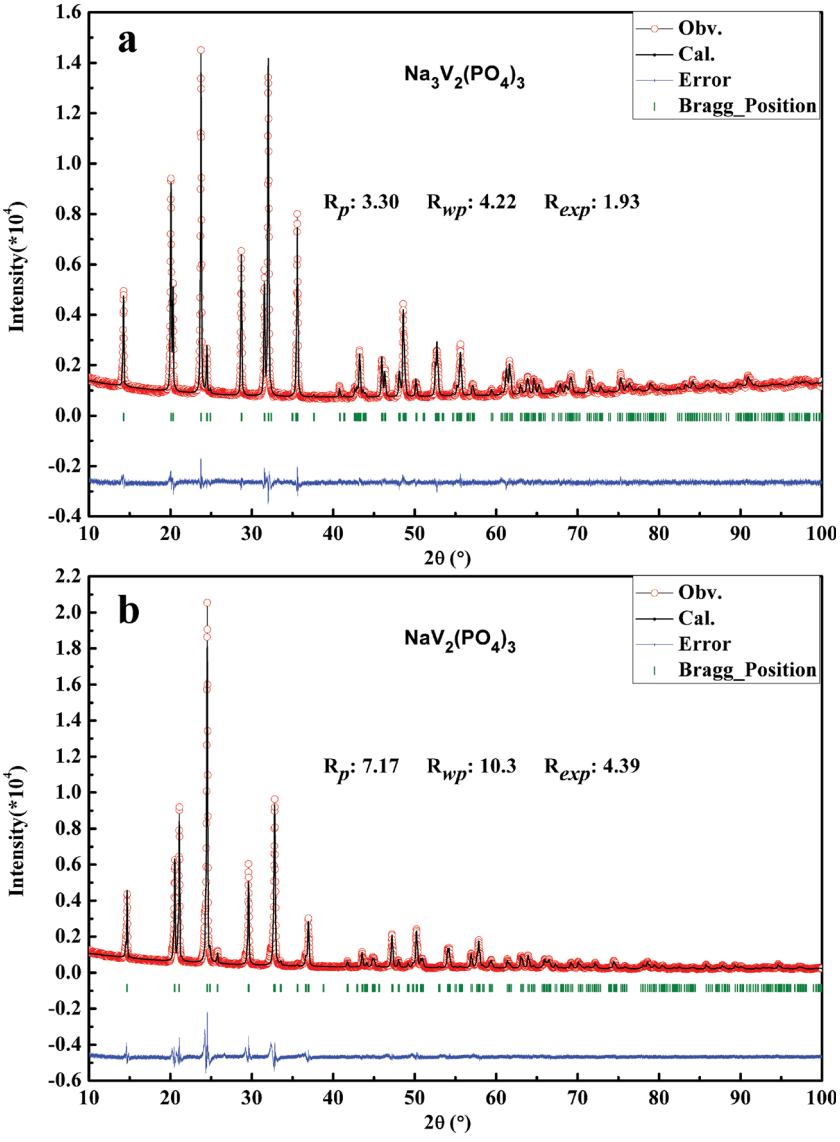


**Figure 1.** Rietveld refined XRD patterns of (a) $Na_3V_2(PO_4)_3$ and (b) $NaV_2(PO_4)_3$.

**Table 1.** Crystallographic data of the $Na_3V_2(PO_4)_3$ at room temperature.

| Atom | Type | Wyckoff | X/a | Y/b | Z/c | Occupancy |
|---|---|---|---|---|---|---|
| Na1 | Na | 6b | 0.00000 | 0.00000 | 0.00000 | 0.8430 |
| Na2 | Na | 18e | 0.63337 | 0.00320 | 0.25000 | 0.7190 |
| V | V | 12c | 0.00000 | 0.00000 | 0.14733 | 1.0000 |
| P | P | 18e | 0.29156 | 0.00000 | 0.25000 | 1.0000 |
| O1 | O | 36f | 0.17799 | –0.02933 | 0.19293 | 1.0000 |
| O2 | O | 36f | 0.19171 | 0.16527 | 0.08979 | 1.0000 |

that Na is extracted from the 18e sites. The occupancy rate in $NaV_2(PO_4)_3$ is higher compared with the $Na_3V_2(PO_4)_3$, which may be due to partial Na located at M2 sites moves to M1 sites upon Na extraction. In general, Na is extracted from M2 sites, whereas Na posited at M1 sites is remained.

### 2.2. Aberration-Corrected STEM

In order to directly investigate the atomic positions of Na, aberration-corrected STEM was carried out. **Figures 2**a and b show the schematic diagram of the unit structures for $Na_3V_2(PO_4)_3$ and $NaV_2(PO_4)_3$, respectively, which are deduced from Rietveld refined-XRD. In $NaV_2(PO_4)_3$, there is only one sodium occupancy site (M1), which is located at the shoulder of ellipse. In $Na_3V_2(PO_4)_3$, two different Na sites are located at M1 and M2. Sodium atoms in M2 should be located at inside the ellipse and at both sides of the ellipse's tips, as shown in Figure 2a. High-angle annular dark field (HAADF)-STEM images of $Na_3V_2(PO_4)_3$ and $NaV_2(PO_4)_3$ along the $[1\bar{1}\bar{1}]$ projection are shown in Figures 2c and d, respectively. The phosphorus and vanadium atoms can clearly be visible. The patterns are in good agreement with the schematic diagram of structure, indicating that $Na_3V_2(PO_4)_3$ and $NaV_2(PO_4)_3$ have the same cage construction. On the basis of this observation, it is very clear that after Na extraction, the skeleton NASICON structure keeps very well. However, the sodium atom cannot be observed in the HAADF-STEM images. The information of Na atomic positions can be observed in the ABF-STEM images. Figures 2e–h show the ABF-STEM images of $Na_3V_2(PO_4)_3$, $NaV_2(PO_4)_3$ along the $[1\bar{1}\bar{1}]$ projection, and their corresponding line profiles. The patterns are the same as those in the HAADF-STEM images. Only one sodium occupancy position is found in $NaV_2(PO_4)_3$, whereas two different positions exist in $Na_3V_2(PO_4)_3$. In both $Na_3V_2(PO_4)_3$ and $NaV_2(PO_4)_3$ samples, Na atoms occupying 6b sites can be visible (marked by yellow circles in the Figures 2e,f). In the ABF-STEM image of $NaV_2(PO_4)_3$, no Na is occupying the M2 sites, whereas Na can be visible in the ABF-STEM image of $Na_3V_2(PO_4)_3$. This analysis is in accordance with the refined-XRD results. Each NASICON structural unit can accommodate four Na atoms, wherein one is located at M1 sites and another three are located at M2 sites. In the ABF-STEM image of $Na_3V_2(PO_4)_3$, the sodium occupying the inside of the ellipse can be clearly visualized (shown in the blue circles and identified by blue arrows). The sodium occupying both sides of ellipse's tips can not obviously be visualized. Therefore, we study the corresponding line profiles, and the image contrast of the dark dots are inverted and displayed as peaks. The result shows one, rather than two, obvious peak of sodium atoms. Nevertheless, no peak can be found in the corresponding sites of $NaV_2(PO_4)_3$. This observation is in good agreement with the refined-XRD results, which indicates that the occupancy rate of M2 sites is only 0.7190, implying numerous vacancies and that Na atoms would not completely fill the M2 sites of $Na_3V_2(PO_4)_3$. In addition, the Na atoms are not randomly distributed in the M2 sites but are possibly distributed in ordering locally for $Na_3V_2(PO_4)_3$. In $Na_3V_2(PO_4)_3$, the distances between the P peak and nearest P/O peak are different: 0.45 and 0.61 nm for d1 and d2, respectively. The occupation of Na atoms in the M2 sites between the P atoms and nearest P/O atoms increase the distance. In addition, the distances between the P peak and nearest P/O peak are the same in $NaV_2(PO_4)_3$, that is, 0.41 nm (d3 = d4), which is less than the distances in $Na_3V_2(PO_4)_3$. To further confirm this interesting phenomenon, a larger area of the ABF-STEM image of $Na_3V_2(PO_4)_3$ is shown in Figure S4. The same behavior is observed. When $Na_3V_2(PO_4)_3$ transfers to $NaV_2(PO_4)_3$, Na atoms occupying M2 sites are extracted from the NASICON structure, whereas other Na atoms remain at M1 sites.

### 2.3. NMR Spectroscopy

NMR spectroscopy was also employed to further understand the sodium kinetics in $Na_xV_2(PO_4)_3$. **Figure 3**a presents the room temperature $^{23}Na$ (spin $I = 3/2$) static spectrum for the

**Table 2.** Crystallographic data of the $NaV_2(PO_4)_3$ at room temperature.

| Atom | Type | Wyckoff | X/a | Y/b | Z/c | Occupancy |
|---|---|---|---|---|---|---|
| Na1 | Na | 6b | 0.00000 | 0.00000 | 0.00000 | 0.9448 |
| V | V | 12c | 0.00000 | 0.00000 | 0.14487 | 1.0000 |
| P | P | 18e | 0.28547 | 0.00000 | 0.25000 | 1.0000 |
| O1 | O | 36f | 0.17236 | –0.02477 | 0.19146 | 1.0000 |
| O2 | O | 36f | 0.18986 | 0.16261 | 0.08717 | 1.0000 |

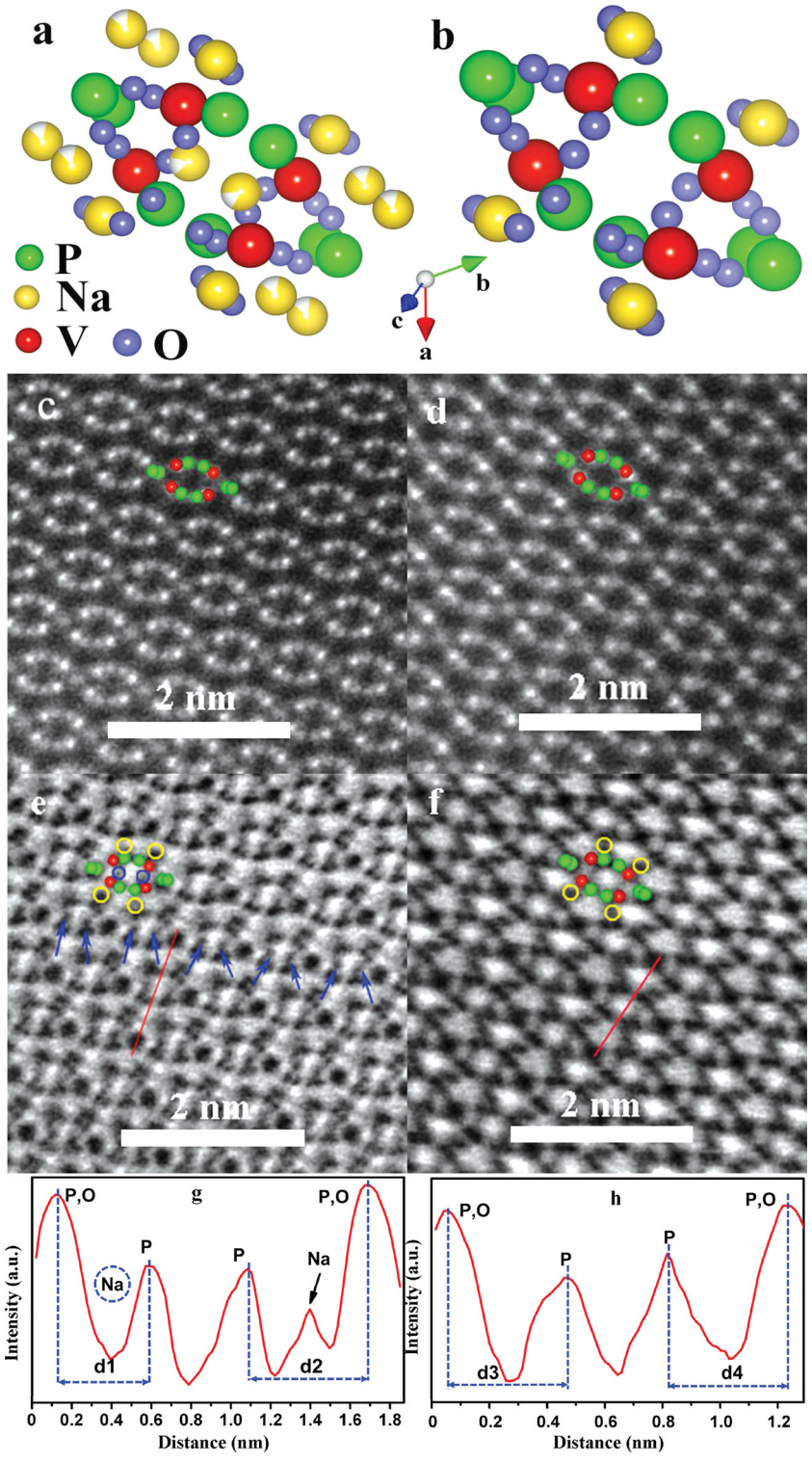


**Figure 2.** Schematic diagram of Structure for (a) $Na_3V_2(PO_4)_3$ and (b) $NaV_2(PO_4)_3$; STEM HAADF images of (c) $Na_3V_2(PO_4)_3$ and (d) $NaV_2(PO_4)_3$ along the $[1\bar{1}\bar{1}]$ projection; STEM ABF images of (e) $Na_3V_2(PO_4)_3$ and f. $NaV_2(PO_4)_3$ along the $[1\bar{1}\bar{1}]$ projection (blue and yellow circles are Na atoms at M1 and M2 sites respectively, blue arrow indicates the Na atoms at M2 site.); line profiles along in the ABF images of g. $Na_3V_2(PO_4)_3$ and h. $NaV_2(PO_4)_3$. In the ABF line profiles, the images contrast of the dark dot are inverted and displayed as peaks.

$Na_3V_2(PO_4)_3$ powder; this spectrum is broad and featureless, approximately Lorentzian line shape with a full width ($\Delta\nu$) at half magnitude (FWHM) of 30 kHz, which corresponds to the central transitions ($m = 1/2 \leftrightarrow -1/2$). Whereas the $m = \pm 3/2 \leftrightarrow \pm 1/2$ satellite transitions are not observed here, possibly due to the distributions of quadrupolar interactions (site distributions at Na site, according to ABF-STEM analysis) that cause the satellite peaks to be smeared out. For $^{23}Na$ nucleus with a mediate quadrupole moment, central lines are primarily broadened from various contributions associated with dipolar, quadrupolar interactions, anisotropic chemical shielding, paramagnetic hyperfine interactions or their distributions. Dipolar interactions, first order quadrupolar interactions, chemical shift anisotropies, and magnetic hyperfine couplings associated with second rank tensors, can be averaged out by magic angle spinning (MAS). Figures 3b and 3c show the room temperature $^{23}Na$ MAS spectra for $Na_3V_2(PO_4)_3$ and $NaV_2(PO_4)_3$, respectively. In Figure 3a, we can see that the static spectrum is overlapped by two components from two non-equivalent Na sites (M1 and M2), whereas in Figures 3b and S5, the MAS spectrum clearly exhibits two distinct peaks attributed to non-equivalent occupancies of $^{23}Na$. The stronger peak positioned at 79 ppm corresponds to two Na atoms bonded to a triangular prism site (M2), and the peak at -9 ppm corresponds to one Na atom at the octahedral site (M1).[16] This line assignment can be simply justified by the analysis of line intensity, coordination numbers (CN) at corresponding crystallographic sites and the temperature dependency of MAS line shape. The octahedral Na site, M1, is coordinated by six oxygen ions connected to six V ions in M1 sites while it is eight oxygen ions at M2 sites. With the different local chemical and topological environments, $Na^+$ ions will exhibit distinct nucleus spin dynamic behaviors, which can be shown in **Figure 4**c and d that the position and width of the M2 peak is significantly affected by heating while it is not the case for M1 peak. Furthermore, the line assignment based on intensity is also in accordance with electrochemical behaviors.[3b] Figure 3c shows the $^{23}Na$ central line splitting of $NaV_2(PO_4)_3$, which is a signature of change of the local chemical environments and/or sub-lattice distortion that occurs at the M1 sites upon the extraction of $Na^+$ from $Na_3V_2(PO_4)_3$, consistent with the results of the Rietveld refined-XRD and ABF-STEM.

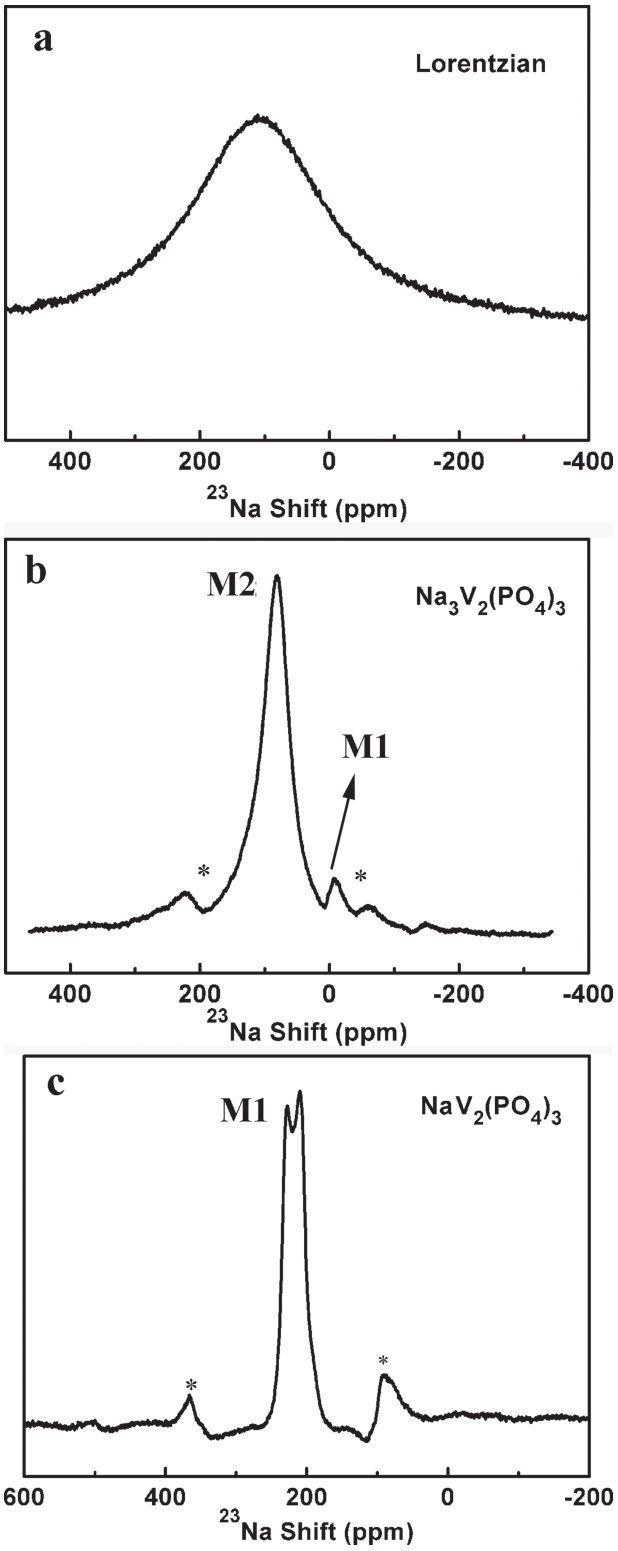


**Figure 3.** a) $^{23}$Na NMR powder spectra of $Na_3V_2(PO_4)_3$ measured at room temperature. Static spectra were fitted by SIMPSON, yielding dipolar coupling constants, isotropic chemical shifts and EFGs. The long range structural ordering probed in X-ray diffraction agrees with the static quadrupolar and dipolar interactions observed for Na nuclei from the NMR data. b,c) The $^{23}$Na MAS spectra for $Na_3V_2(PO_4)_3$ and $NaV_2(PO_4)_3$ recorded at the spinning rate of 14 kHz at 298 K.

To examine the oxidation states of vanadium centers and better understand the local structural features at the Na sites, the electronic and magnetic properties were further investigated by NMR and superconducting quantum interference device (SQUID) at various temperatures. Figure 4a shows the temperature dependence of magnetic susceptibilities ($\chi$) for both as-prepared $Na_3V_2(PO_4)_3$ and $NaV_2(PO_4)_3$ compounds. Their paramagnetic parts of temperature dependence follow the Curie-Weiss law (C-W): $\chi^{-1} = (T+\theta)/C$, where $\theta$ is Weiss temperature and C is Curie constant. Linear least-square root fittings yield $\theta$ = 26 K and $C$ = 2.2 emu K/Oe-f.u. for $Na_3V_2(PO_4)_3$, while $\theta$ = –112 K and $C$ = 1.2 emu K/Oe-f.u. for $NaV_2(PO_4)_3$ compound. Effective magnetic moments for V ions can thus be obtained from Curie constants of 3.1 $\mu_B$ and 1.9 $\mu_B$ for $Na_3V_2(PO_4)_3$ and $NaV_2(PO_4)_3$, respectively.[17] These values are roughly close to the $V^{3+}$ spin with value of 2.83 $\mu_B$ ($C_{theo}$ = 1 with $3d^2$ and S = 1) and $V^{4+}$ of 1.5 $\mu_B$. In this material, the clear change of V oxidation states upon Na extraction suggests the capacity as the redox of vanadium center in this material. Figure 4b shows the linear dependence of $^{23}$Na NMR isotropic shifts versus magnetic susceptibility. Linear fittings yield positive hyperfine fields: $zH_{hf}^{sd}$ = 54 kOe/$\mu_B$ at the M2 sites in $Na_3V_2(PO_4)_3$ and 253 kOe/$\mu_B$ at the M1 sites in $NaV_2(PO_4)_3$ compounds, respectively. The shift in $Na_3V_2(PO_4)_3$ extrapolated to $\chi^{CW} = 0$ is 32 ± 5 ppm. This difference in hyperfine fields is in good agreement with their chemical environments where the oxidation state of vanadium centers coordinated with Na at M1 sites is higher than those coordinated with Na at M2 sites. The isotropic shift can be described by $\delta_{iso} = \delta_{cs} + \delta_{sd}$ (T), where $\delta_{cs}$ is the chemical shift ascribed to chemical shielding. $\delta_{sd}$ is the shift originating from the transferred hyperfine interactions with local magnetic moments of neighboring V ions due to *s-d* exchange polarization. Transfer of electron density from the $V^{3+}$ $t_{2g}$-like orbitals to the Na 3*s* orbital gives rise to a positive shift (delocalization mechanism). The above analysis on local environments and shift mechanisms explains the observed larger $^{23}$Na shift at M2 site than that at M1 site. Similar paramagnetic effects on $^{6,7}$Li NMR shifts have been observed in lithium-ion batteries.[18]

The analysis of MAS central line width data is non-trivial since the MAS spectra might be superposition of two components, such as second order quadrupolar and anisotropic paramagnetic broadening.[19] In paramagnetic samples, the distribution of isotropic part of bulk magnetic susceptibility only results in a line broadening of the resonance but no overall the isotropic shift. The anisotropic line broadening in paramagnetic materials was considered to have a similar mechanism as second order quadrupolar coupling,[20] which turns out to be very small under fast MAS.[6,21] In contrast to line shift, the broadening of the $^{23}$Na NMR spectra grows non-linearly with respect to $\chi$ unexpected from magnetic broadening mechanisms, thereby indicating a linear relation between $^{23}$Na shifts versus line width,[22] as shown in Figure 4c. Thus, the temperature dependence of MAS line width opens another possibility of the onset of atomic motion on a timescale comparable to the reciprocal of linewidth (in Hz) broadened by second order quadrupole interactions.[23] The MAS central linewidth ($\Delta\nu$) broadened by second order quadruple interaction can be described as:[24] $\nu_0\Delta\upsilon = 25C_Q^2/192$ for $^{23}$Na nuclear spin

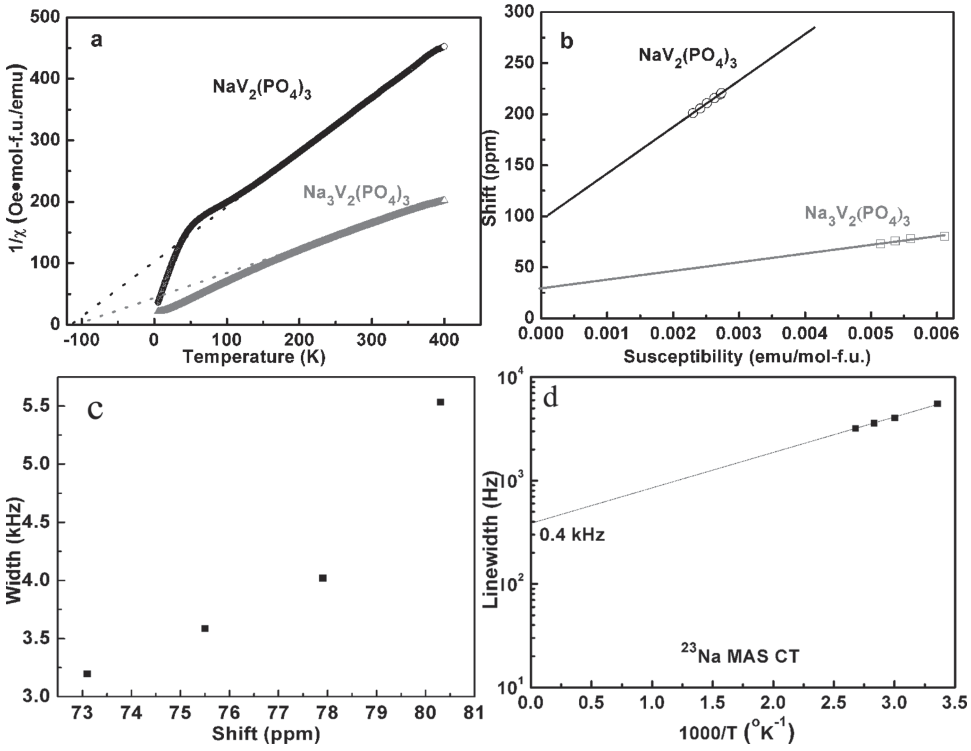


**Figure 4.** a) $K_{iso}$ versus $\chi$ with temperature as an implicit parameter. All susceptibilities were normalized per mole of the formula unit, while the effective magnetic moments of V were calculated using $\mu_{eff} = 1/2^*(8C)^{1/2}$. b) The linear dependence of $^{23}$Na NMR isotropic shift versus magnetic susceptibility. c) $^{23}$Na shifts versus line width of $Na_3V_2(PO_4)_3$. d) Temperature dependence of full line width at half height $^{23}$Na linewidth for $Na_3V_2(PO_4)_3$ sample.

($I = 3/2$), where $\nu_0$ is Larmor frequency and $C_Q$ is quadrupole coupling constant. The thermal motion of $Na^+$, which is directionally bonded in a group, will rotate or liberate the Na-O bond between the ion and its surrounding neighbors and hence decrease $C_Q$.[25] For simplicity, we treat the occupied M2 as a point defect. In this case, the spatial symmetry of a point-charge quadrupolar interaction is identical to that of the dipolar interaction.[26] For thermally activated process of atomic motions in solid states, the correlation time for ions resident on a lattice follows the Arrhenius equation:[27] $\Delta\nu = Ae^{-E_a/RT}$, where A is a pre-exponential factor and $E_a$ is the activation energy. For a range of correlation times as a function of temperature, broadening behavior should appear when the system approaches the condition: $\omega_1\tau_c \approx 1$. In the $\omega_1\tau_c 1$ regime for this case (weakly collision within the investigated temperature range), by plotting the logarithm of linewidth versus $1/T$ (in Kelvin), it can immediately be seen the slope of the linear part of the line should be the activation energy $E_a$, as shown in Figure 4d. Thus, the temperature dependence of linewidth can be described in terms of a thermally activated hopping process with very low activation energy of 6.8 kJ/mol (~0.1 eV), much smaller than that in other NASICON compounds.[28] For the $Na^+$ ion extracted compound, $NaV_2(PO_4)_3$, where Na resides in M1 sites, $\Delta\nu$ remains almost constant in the temperature range of 295 ≤T ≤ 375 K (as shown in **Figure 5**), as expected from the fact that the $Na^+$ ion coordination environment at the M1 sites (CN = 6) is different from that at the M2 sites (CN = 8) (also see **Figure 6**).[29] $Na^+$ ions are mostly entrapped in the M1 sites due to the shorter average Na-O bond length and smaller polyhedral volume than those of M2 sites (Table S3), thereby demonstrating the structural effects on the mobility of ions.[2c,3a,28a] Dynamic behaviors show that the $Na^+$ ions tend to remain immobilized in the M1 sites, whereas those ions in the M2 sites become mobile via a M2-M2 sodium-transport mechanism within the investigated temperatures, which are in good agreement with the report of Goodenough.[3a]

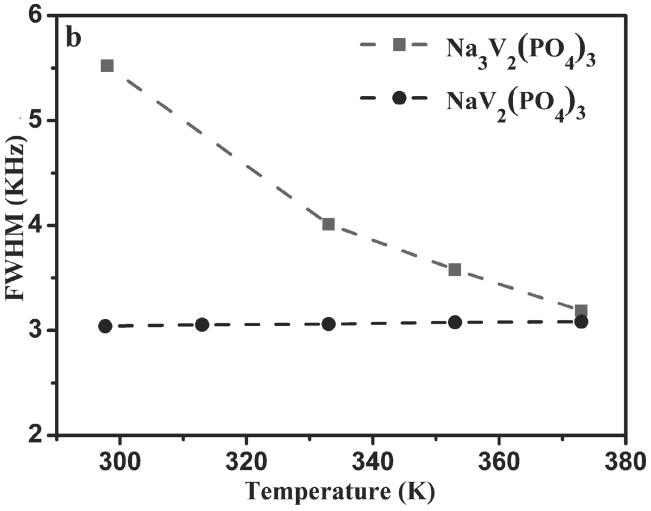


**Figure 5.** FWHM at different temperatures of main peaks for $^{23}$Na NMR in the $Na_3V_2(PO_4)_3$ and $NaV_2(PO_4)_3$ samples.

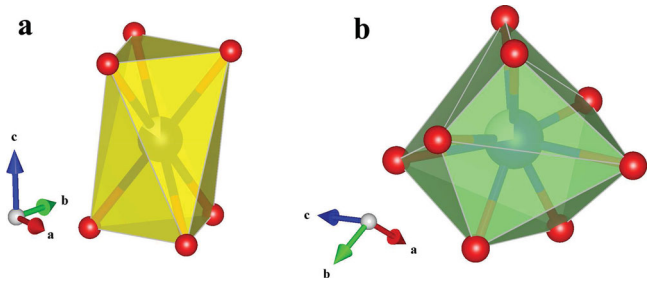


**Figure 6.** Polyhedral structures of M1 site (a) and M2 site (b) from the crystal structure of $Na_3V_2(PO_4)_3$, red ball is oxygen, blue ball is sodium.

## 3. Conclusions

We investigate the $Na^+$ ion positions at atomic resolution and their kinetics to further understand the mechanism of sodium storage in $Na_3V_2(PO_4)_3$. Combined with Rietveld refined-XRD, ABF-STEM, and NMR, we have confirmed that there are two different types of Na sites (6b, M1 and 18e, M2) with different coordination environments in $Na_3V_2(PO_4)_3$, while there is only one type of Na site (6b, M1) in $NaV_2(PO_4)_3$. In addition, in $Na_3V_2(PO_4)_3$, the Na atoms are not randomly distributed in M2 sites, but possibly in an ordered arrangement locally. When Na is extracted from $Na_3V_2(PO_4)_3$ to form $NaV_2(PO_4)_3$, $Na^+$ ion located at the M2 site is extracted and the rest of Na remain at M1 site. NMR analysis indicates that $Na^+$ ion at the M2 sites in $Na_3V_2(PO_4)_3$ is mobile whereas $Na^+$ ion at the M1 site is immobile, suggesting a direct M2 to M2 conduction pathway. Only Na at the M2 sites can be extracted at room temperature, corresponding to about two Na extraction from the $Na_3V_2(PO_4)_3$ structure while its skeleton structure still remains well, which is consistent with the experimental observation of a capacity of 107 mAh/g and excellent cycling performance.

## 4. Experimental Section

The rhombohedral $Na_3V_2(PO_4)_3$ compound was synthesized by mixing stoichiometric amount of $NaH_2PO_4$ (Aldrich, 99.6%) and $V_2O_3$ (Aldrich, 98+%). Chemically sodium extraction of the sample was accomplished by reaction with a strong oxidant nitronium tetrafluoroborate ($NO_2BF_4$, Aldrich, 98%). Different molar ratio of $NO_2BF_4$: $Na_3V_2(PO_4)_3$ was selected. More details of experiments are described in our previous reports.[3b,4]

The structural characterization was performed using an X'Pert Pro MPD X-ray diffractometer (Philips, Netherlands) with Cu K$\alpha$ radiation (1.5405 Å). The aberration-corrected scanning transmission electron microscopy (STEM) was performed using a JEOL 2100F (JEOL, Tokyo, Japan) transmission electron microscope operated at 200 keV. The microscope is equipped with a CEOS (CEOS, Heidelberg, Germany) probe aberration corrector. The attainable spatial resolution of the microscope is 90 picometer at an incident semiangle of 20 mrad. To observe Na directly using ABF collection geometry, the acceptance semiangle in this study was fixed between 10–20 mrad. The NMR spectra were measured in the temperature range between 295 and 373 K with a Bruker ADVANCE III spectrometer operating at a magnetic field of 9.39 T. The chemical shift reference is NaCl powder (7.3 ppm). Susceptibility measurements were taken with a Quantum Design MPMS SQUID magnetometer between 5 and 400 K. Data were taken with the samples cooled in the absence of an applied field (zero-field cooled) and in the measuring field (field cooled at 1 Tesla).

## Supporting Information

Supporting Information is available from the Wiley Online Library or from the author.

## Acknowledgements

Z.L.J. and C.C.Y. contributed equally to this work. The authors thank Huilin Pan, Yuesheng Wang and Yang Sun for helpful discussion. This work was supported by funding from "973" Projects (2010CB833102, 2012CB932900), NSFC (No. 51222210, 51071171, 11234013, 11174334, 11205249), and the 100 Talent Project of the Chinese Academy of Sciences.

Received: January 17, 2014
Revised: February 17, 2014
Published online: April 2, 2014

[1] a) H. Pan, Y.-S. Hu, L. Chen, *Energy Environ. Sci.* **2013**, *6*, 2338; b) S. W. Kim, D. H. Seo, X. Ma, G. Ceder, K. Kang, *Adv. Energy Mater.* **2012**, *2*, 710; c) M. D. Slater, D. Kim, E. Lee, C. S. Johnson. *Adv. Funct. Mater.* **2012**, *23*, 947; d) V. Palomares, P. Serras, I. Villaluenga, K. B. Hueso, J. Carretero-González, T. Rojo, *Energy Environ. Sci.* **2012**, *5*, 5884.

[2] a) S. Komaba, W. Murata, T. Ishikawa, N. Yabuuchi, T. Ozeki, T. Nakayama, A. Ogata, K. Gotoh, K. Fujiwara, *Adv. Funct. Mater.* **2011**, *21*, 3859; b) J. M. Zhao, Z. L. Jian, J. Ma, F. C. Wang, Y. S. Hu, W. Chen, L. Q. Chen, H. Z. Liu, S. Dai, *ChemSusChem* **2012**, *5*, 1495; c) B. L. Ellis, W. R. M. Makahnouk, Y. Makimura, K. Toghill, L. F. Naza, *Nature Mater.* **2007**, *6*, 749; d) Y. Sun, L. Zhao, H. Pan, X. Lu, L. Gu, Y.-S. Hu, H. Li, M. Armand, Y. Ikuhara, L. Chen, X. Huang, *Nat. Commun.* **2013**, *4*, 1870; e) H. Pan, X. Lu, X. Yu, Y.-S. Hu, H. Li, X.-Q. Yang, L. Chen, *Adv. Energy Mater.* **2013**, *3*, 1186; f) L. Zhao, J. Zhao, Y. S. Hu, H. Li, Z. Zhou, M. Armand, L. Chen, *Adv. Energy Mater.* **2012**, *2*, 962; g) Y. Cao, L. Xiao, W. Wang, D. Choi, Z. Nie, J. Yu, L. V. Saraf, Z. Yang, J. Liu, *Adv. Mater.* **2011**, *23*, 3155; h) Y. Wang, X. Yu, S. Xu, J. Bai, R. Xiao, Y.-S. Hu, H. Li, X.-Q. Yang, L. Chen, X. Huang, *Nat. Commun.* **2013**, *4*, 2365; i) Y.-U. Park, D.-H. Seo, H.-S. Kwon, B. Kim, J. Kim, H. Kim, I. Kim, H.-I. Yoo, K. Kang, *J. Am. Chem. Soc.* **2013**, *135*, 13870.

[3] a) B. L. Cushing, J. B. Goodenough, *J. Solid State Chem.* **2001**, *162*, 176–181; b) Z. Jian, L. Zhao, H. Pan, Y.-S. Hu, H. Li, W. Chen, L. Chen, *Electrochem. Commun.* **2012**, *14*, 86.

[4] Z. Jian, W. Han, X. Lu, H. Yang, Y.-S. Hu, J. Zhou, Z. Zhou, J. Li, W. Chen, D. Chen, L. Chen, *Adv. Energy Mater.* **2013**, *3*, 156.

[5] H. Kabbour, D. Coillot, M. Colmont, C. Masquelier, O. Mentré, *J. Am. Chem. Soc.* **2011**, *133*, 11900.

[6] J. Kim, D. S. Middlemiss, N. A. Chernova, B. Y. X. Zhu, C. Masquelier, C. P. Grey, *J. Am. Chem. Soc.* **2010**, *132*, 16825.

[7] a) H. Yu, S. Guo, M. Ishida, Y. Zhu, H. Zhou, *Chem. Commun.* **2014**, *50*, 457; b) P. Ballirano, R. Caminiti, *J. Appl. Crystallogr.* **2001**, *34*, 757.

[8] a) P. Gibot, M. Casas-Cabanas, L. Laffont, S. Levasseur, P. Carlach, S. Hamelet, J. M. Tarascon, C. Masquelier, *Nat. Mater.* **2008**, *7*, 741; b) X. Yu, H. Pan, W. Wan, C. Ma, J. Bai, Q. Meng, S. Ehrlich, Y.-S. Hu, X.-Q. Yang, *Nano Lett.* **2013**, *13*, 4721; c) N. Yabuuchi, M. Kajiyama, J. Iwatate, H. Nishikawa, S. Hitomi, R. Okuyama, R. Usui, Y. Yamada, S. Komaba, *Nat. Mater.* **2012**, *11*, 512; d) R. Berthelot, D. Carlier, C. Delmas, *Nat. Mater.* **2010**, *10*, 74.

[9] a) L. Gu, C. Zhu, H. Li, Y. Yu, C. Li, S. Tsukimoto, J. Maier, Y. Ikuhara, *J. Am. Chem. Soc.* **2011**, *133*, 4661; b) L. Suo, W. Han, X. Lu, L. Gu, Y.-S. Hu, H. Li, D. Chen, L. Chen, S. Tsukimoto, Y. Ikuhara, *Phys. Chem. Chem. Phys* **2012**, *14*, 5363.

[10] a) X. Lu, L. Zhao, X. He, R. Xiao, L. Gu, Y.-S. Hu, H. Li, Z. Wang, X. Duan, L. Chen, J. Maier, Y. Ikuhara, *Adv. Mater.* **2012**, *24*, 3233; b) Y.-Q. Wang, L. Guo, Y.-G. Guo, H. Li, X.-Q. He, S. Tsukimoto, Y. Ikuhara, L.-J. Wan, *J. Am. Chem. Soc.* **2012**, *134*, 7874.
[11] X. Lu, Y. Sun, Z. Jian, X. He, L. Gu, Y.-S. Hu, H. Li, Z. Wang, W. Chen, X. Duan, *Nano Lett.* **2012**, *12*, 6192.
[12] a) Y. Xia, N. Machida, X. H. Wu, C. Lakeman, L. van Wullen, F. Lange, C. Levi, H. Eckert, *J. Phys. Chem. B* **1997**, *101*, 9180; b) L. S. Cahill, R. P. Chapman, C. W. Kirby, G. R. Goward, *Appl. Magn. Reson.* **2007**, *32*, 565; c) H. D. Morris, S. Bank, P. D. Ellis, *J. Phys. Chem.* **1990**, *94*, 3121–3129; d) A. Castets, D. Carlier, K. Trad, C. Delmas, M. Menetrier, *J. Phys. Chem. C* **2010**, *114*, 19141.
[13] a) J. Gopalakrishnan, K. K. Rangan, B. R. Prasad, C. K. Subramanian, *J. Solid State Chem.* **1994**, *111*, 41; b) G. Rousse, J. Rodriguez-Carvajal, C. Wurm, C. Masquelier, *Chem. Mater.* **2001**, *13*, 4527; c) L. J. M. Davis, X. J. He, A. D. Bain, G. R. Goward, *Solid State Nucl. Magn. Reson.* **2012**, *42*, 26.
[14] N. A. Chernova, G. M. Nolis, F. O. Omenya, H. Zhou, Z. Li, M. S. Whittingham, *J. Mater. Chem.* **2011**, *21*, 9865.
[15] a) S. Susman, C. J. Delbecq, T. O. Brun, E. Prince, *Solid State Ionics* **1983**, *9–10*, 839; b) J. P. Boilot, G. Collin, P. Colomban, *J. Solid State Chem.* **1988**, *73*, 160; c) J. Gopalakrishnan, K. K. Rangan, *Chem. Mater.* **1992**, *4*, 745.
[16] I. V. Zatovsky, *Acta Crystallog. E* **2010**, *66*, I12.
[17] J. Li, M. E. Lashier, G. L. Schrader, B. C. Gerstein, *Appl. Catalysis* **1991**, *73*, 83.
[18] a) S. C. Yin, H. Grondey, P. Strobel, H. Huang, L. F. Nazar, *J. Am. Chem. Soc.* **2003**, *125*, 326; b) N. Dupre, J. Gaubicher, D. Guyomard, C. P. Grey, *Chem. Mater.* **2004**, *16*, 2725.
[19] L. Li, Y. Wu, *J. Chem. Phys.* **2008**, *128*, 052307.
[20] A. R. Brough, C. P. Grey, C. M. Dobson, *J. Am. Chem. Soc.* **1993**, *115*, 7318.
[21] a) A. K. Cheetham, C. M. Dobson, C. P. Grey, R. J. B. Jakeman, *Nature* **1987**, *328*, 706; b) N. P. Wickramasinghe, M. Shaibat, Y. Ishii, *J. Am. Chem. Soc.* **2005**, *127*, 5796; c) J. F. Colin, T. Bataille, S. E. Ashbrook, N. Audebrand, L. Le Polles, J. Y. Pivan, E. Le Fur, *Inorg. Chem.* **2006**, *45*, 6034.
[22] D. E. MacLaughlin, O. O. Bernal, H. G. Lukefahr, *J. Phys.-Condens. Matter* **1996**, *8*, 9855.
[23] N. A. Sergeev, A. M. Panich, M. Olszewski, *Appl. Magn. Reson.* **2004**, *27*, 41.
[24] C. P. Slichter, Principles of Magnetic Resonance, Springer, New York **1996**.
[25] a) D. T. Amm, S. L. Segel, K. R. Jeffrey, *Can. J. Phys.* **1986**, *64*, 22; b) J. W. Akitt, *Prog. Nucl. Magn. Reson. Spectrosc.* **1989**, *21*, 1–149; c) A. V. Sapiga, N. A. Sergeev, *Cryst. Res. Technol.* **2001**, *36*, 875.
[26] W. W. Warren, *Phys. Rev. A* **1974**, *10*, 657.
[27] D. S. Schreiber, R. M. Cotts, *Phys. Rev.* **1963**, *131*, 1118.
[28] a) A. Martinez-Juarez, C. Pecharroman, J. E. Iglesias, J. M. Rojo, *J. Phys. Chem. B* **1998**, *102*, 372; b) C. M. Chang, S. H. Hong, H. M. Park, *Solid State Ionics* **2005**, *176*, 2583.
[29] A. M. Glass, K. Nassau, *J. Appl. Phys.* **1980**, *51*, 3756.